SPECIAL ISSUE ARTICLE

JOR Spine OPEN ACCESS

Spatial mapping of collagen content and structure in human intervertebral disk degeneration

Lawrence Zeldin[1] | Grace E. Mosley[1] | Damien Laudier[1] |
Zachary S. Gallate[1] | Jennifer Gansau[1] | Robert C. Hoy[1] |
Jashvant Poeran[1,2] | James C. Iatridis[1]

[1]Leni & Peter W. May Department of Orthopedics, Icahn School of Medicine at Mount Sinai, New York, New York

[2]Department of Population Health Science and Policy, Icahn School of Medicine at Mount Sinai, New York, New York

Correspondence
James C. Iatridis, Leni & Peter W. May Department of Orthopaedics, Icahn School of Medicine at Mount Sinai, 1 Gustave Levy Place, Box 1188, New York, NY 10029-6574.
Email: james.iatridis@mssm.edu

Abstract

Collagen plays a key structural role in both the annulus fibrosus (AF) and nucleus pulposus (NP) of intervertebral disks (IVDs). Changes in collagen content with degeneration suggest a shift from collagen type II to type I within the NP, and the activation of pro-inflammatory factors is indicative of fibrosis throughout. While IVD degeneration is considered a fibrotic process, an increase in collagen content with degeneration, reflective of fibrosis, has not been demonstrated. Additionally, changes in collagen content and structure in human IVDs with degeneration have not been characterized with high spatial resolution. The collagen content of 23 human lumbar L2/3 or L3/4 IVDs was quantified using second harmonic generation imaging (SHG) and multiple image processing algorithms, and these parameters were correlated with the Rutges histological degeneration grade. In the NP, SHG intensity increased with degeneration grade, suggesting fibrotic collagen deposition. In the AF, the entropy of SHG intensity was reduced with degeneration indicating increased collagen uniformity and suggesting less-organized lamellar structure. Collagen orientation entropy decreased throughout most IVD regions with increasing degeneration grade, further supporting a loss in collagen structural complexity. Overall, SHG imaging enabled visualization and quantification of IVD collagen content and organization with degeneration. There was an observed shift from an initially complex structure to more uniform structure with loss of microstructural elements and increased NP collagen polarity, suggesting fibrotic remodeling.

KEYWORDS

collagen, degeneration, entropy, human, intervertebral disk, second harmonic generation

1 | INTRODUCTION

Low back pain is a major cause of age-associated disability, affecting approximately 632 million people globally[1] and 70% to 85% of US individuals at some point in their lives.[2] Low back pain is responsible for the most years lived with disability of any disease,[2] and US prevalence of this condition is increasing.[3-5] The most common back pain diagnosis is intervertebral disk (IVD) degeneration[6] and specific structural disruptions of the IVD can contribute directly to pain and disability.[7] Thus, better characterization

of human IVD degeneration may improve understanding of the development of back pain.

The IVD is composed of an outer annulus fibrosus (AF) and an inner nucleus pulposus (NP). Much of the structural integrity of the IVD is supplied by the extensive extracellular matrix, of which collagen is a key component.[8-10] The AF consists mainly of type I collagen, oriented in concentric lamellae around the NP in an angle ply structure.[11] The NP is a gelatinous structure composed of proteoglycans, water, and a mesh of type II collagen.[8,12] Moving from outer AF to the NP, the relative composition shifts from predominantly type I to type II collagen as the water and glycosaminoglycan content increase.[8,13-15] Histological characterization of IVD degeneration demonstrated several degenerative changes in the IVD, including macroscopic loss of a clear NP-AF boundary, loss of gel-like properties in the NP, and a disrupted annular structure.[16,17] Reported alterations in NP collagen synthesis and degradation suggest a shift in composition toward increased type I collagen content.[13] However, the collagen content changes in the NP remain unclear. Despite NP degradation commonly being described as a shift from gelatinous to fibrous composition,[17] NP hydroxyproline levels remain constant[13] and NP collagen content decreases with age.[18]

Collagen microstructure in the IVD has been studied extensively and is described in multiple reviews.[10,19] While biochemical studies have characterized compositional changes in the IVD with degeneration,[13,18] changes in collagen structure in human IVD degeneration are not as well described across IVD regions and degenerative grades. Improved spatial and morphological characterization of collagen structure and content in human IVD degeneration is required to determine whether patterns of increased NP fibrosis can distinguish certain IVD degeneration phenotypes and may inform future biomechanical studies and molecular treatments.[20] Further, microscopic analysis of the collagen structure that is sampled systematically across the various IVD regions may shed light on the differences between biochemical studies that suggest a decrease in NP collagen[18] and histological studies that suggest NP fibrosis.[17]

In this study, second harmonic generation (SHG) imaging was used to analyze IVD collagen structure in human samples. SHG is a two-photon microscopic technique that has been exploited previously to image collagen in various tissue types, such as IVD, arterial wall, and tendon.[21] It is a nondestructive imaging method that uses collagen's hyperpolarizability under infrared (IR) light to image its structure with high resolution without the need for staining. The use of SHG imaging to measure various parameters of collagen structure and content has been validated previously by multiple groups by biochemical and histological means, including in IVD tissue.[15,21-27] Although an indirect measure of collagen, SHG can characterize collagen structure and content in a nondestructive manner, allowing future in vivo applications.[25] SHG is specific to noncentrosymmetric molecules, which includes both collagen types I and II, and largely excludes other components of the extracellular matrix.[24,28-30] Thus, SHG signal is affected by alterations in the collagenous network and largely unaffected by the presence of other matrix components such as proteoglycans.[31] There is evidence of a strong correlation between SHG signal intensity and collagen content in hydrogels and IVD tissues[15,23]; ; however, other parameters such as fibril diameter, fibril disorder, and molecular integrity have been shown to affect signal strength as well.[22,23,26] Further, in a study by Reiser et al, it was suggested to use SHG as a means to identify permanent damage in IVDs by characterizing the collagen structural disorder within the disk tissue.[22] However, previous SHG studies on human IVDs have been limited by either focusing on endplate structure[32] or the use IVDs of a single degeneration grade only.[27,33] Thus, there is a need for whole-IVD SHG analysis across different grades to validate the robustness of this technology for IVD degeneration.

The purpose of this study was to use SHG to assess the structure and spatial distribution of collagen across cadaveric human IVD sagittal sections with varying degenerative grades. SHG images were sampled with predefined imaging regions from the anterior AF (aAF), NP, posterior AF (pAF), and transition zones (aT and pT in respect to anterior and posterior transition zones) to identify fibrotic changes in collagen structure with IVD degeneration. The imaging regions were standardized for all samples to allow regions of interest to be selected in an unbiased manner. SHG imaging was used with multiple computational analyses to characterize the morphometric changes, collagen content, and fibrillar organization throughout the human IVD with degeneration. We correlated these parameters with degeneration grade across IVD region to quantify changes in collagen content and structure by IVD region. Lastly, we performed multivariable regression analyses to evaluate the association between degeneration and SHG imaging parameters and determine the role of age in this context. These novel analyses enable determination of refined degenerative microstructural changes to collagen structure in the IVD, providing novel information that informs understanding of IVD pathology and damage.

2 | MATERIALS AND METHODS

2.1 | Human specimens

Human samples were obtained from an institutional biobank of cadaveric IVDs. This study included 23 lumbar L2/3 or L3/4 IVDs (11 Male, 12 Female) (Table 1). The morphological degeneration of each sample was quantified using the Thompson degeneration scale that ranges from grade 1to 5, with 5 as the most degenerated.[34] Each sample's Thompson grade was determined using the average grade (rounded to the nearest integer) of 3 trained and independent graders. Thompson grades were used to ensure samples were selected from all degeneration levels in a balanced manner.

2.2 | Histological analysis

Specimens were fixed in formal in, embedded in resin, and sectioned in the sagittal plane as previously described.[35] Mid-sagittal 5 μm sections from each sample were stained with picrosirius red/alcian blue

TABLE 1 Human autopsy study sample demographics. Thompson morphological degeneration grade, Rutges histological degeneration grade, age, sex and vertebral level of 23 samples used in this study

Thompson grade	Rutges grade	Age/Sex	Vertebral level
1	1.3	28/M	L2/3
	3	30/F	L2/3
2	2.3	58/F	L2/3
	3	22/F	L3/4
	3	24/M	L2/3
	6	54/M	L2/3
3	7	52/M	L3/4
	4.7	66/F	L3/4
	2.7	32/F	L2/3
	9.7	40/M	L2/3
	7.3	74/F	L2/3
4	8.3	47/F	L3/4
	6.3	93/M	L2/3
	7.3	66/F	L2/3
	5.7	85/M	L3/4
	10	79/F	L3/4
	5.3	48/M	L3/4
5	5	62/F	L3/4
	12	85/M	L3/4
	12	85/M	L2/3
	5	81/F	L2/3
	12	83/F	L2/3
	5	72/M	L2/3

(PR/AB) or hematoxylin and eosin (H&E). After staining, histological degeneration grade was quantified using the Rutges degeneration grading scale to generate a better degeneration resolution for SHG analysis. The Rutges scale ranges from 0 to 12, with 12 being the most degenerated.[36] Each sample was graded for Rutges grade by three trained graders who were blinded to the sample age, sex, and to the Thompson grade.

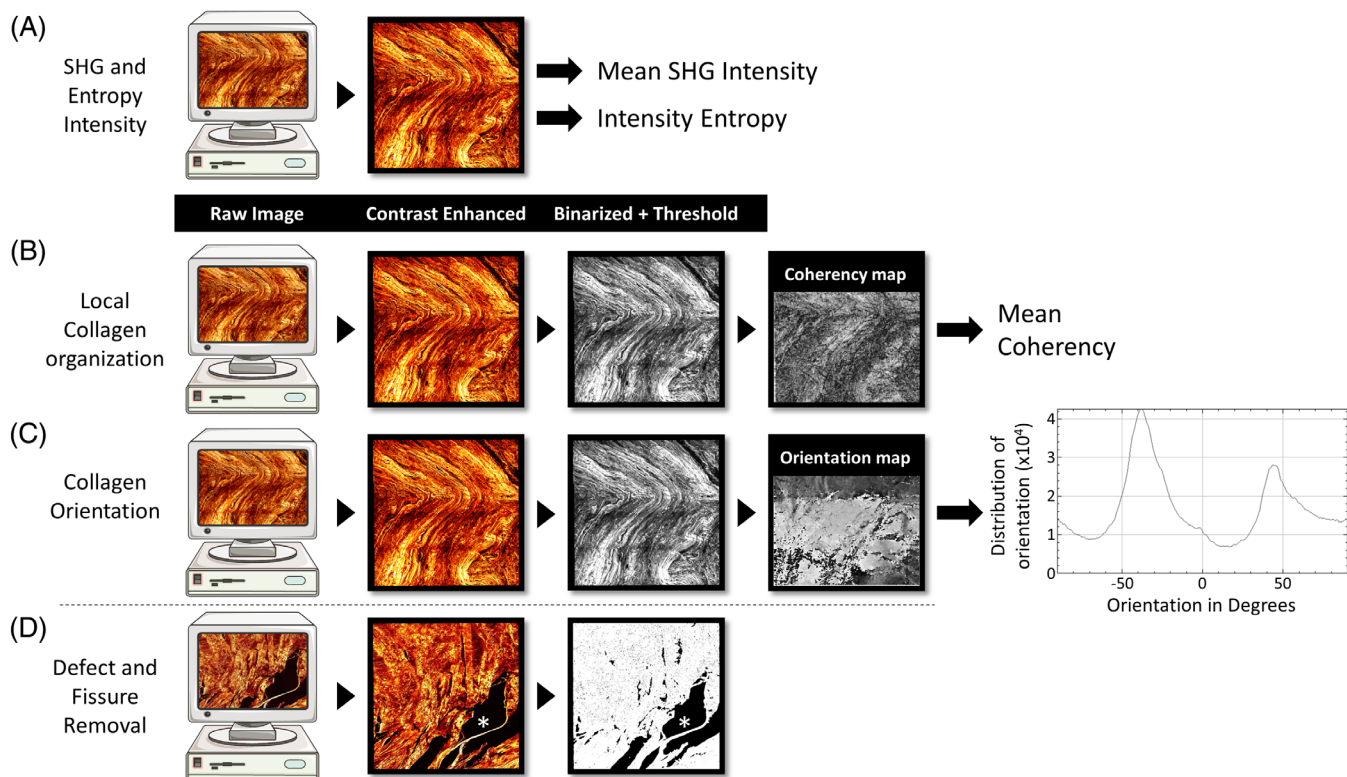## 2.3 | Second harmonic generation imaging

SHG imaging was performed on unstained, de-plasticized sections adjacent to those used for histological grading, using an Olympus FV1000MPE two-photon microscope with 910 nm excitation wavelength (Olympus Corporation, Tokyo, Japan). SHG signal was collected in the backward direction at 25X magnification and photomultiplier tube at 440 ± 20 nm. Images were performed with a step size of 1.5 μm through approximately 10 μm. Imaging resolution was 512 × 512 pixels. A 4 × 4 tiled mosaic was collected at each selected position, with 20% overlap of individual images to minimize artifacts from the tiling protocol. A grid of tiling artifact is still visible, although

this tiling protocol was uniform across all images so it would not affect relative comparisons. A max-intensity z-projection was performed to account for image thickness variation. All images were background subtracted using a 50-pixel rolling-ball radius.

Regions for sample imaging were selected to include the anterior AF, posterior AF, NP, anterior transitional region and posterior transitional region, as follows: midpoints between the superior and inferior IVD borders at the ends of each IVD were selected. The coordinates of these points were used to determine their distance, and a "ruler" was thereby determined, such that the midpoints at the aAF and pAF were positions 0 and 10, respectively. Ten midline images were taken across the section from anterior to posterior to assess collagen structure. Minor vertical translation from midline was permitted only to avoid large histological defects that took up the majority of the image view. This vertical translation was also used to ensure imaging of IVD tissue and not the endplate when analyzing highly degenerated (Thompson grade 5) IVDs. This standardized imaging protocol was established after measuring a subset of samples in the study and choosing positions that would most consistently represent the NP and AF. The location of the transition zone between the NP and AF was variable and sometimes nondiscernable in degenerated IVDs, thus the degree of NP and AF character in the aT and pT imaging zones was variable. We thus analyze these transitional zones separately.

2.4 | Image analysis

Image analysis of SHG images was performed in the FIJI distribution of ImageJ.[37] The OrientationJ[38] plugin was used for binarization and image analysis according to a standardized pipeline. SHG intensity was quantified in FIJI. To determine the degree of collagen content variation in each image, Shannon entropy of the intensity histogram (henceforth referred to as intensity entropy) was measured using a custom written MatLab code (MathWorks, Version R2017a, Massachusetts) (Figure 1A). To analyze the variability of fiber orientations within the image, masked images were contrast enhanced, fibril orientation was calculated with a two-pixel Gaussian window, and orientation plotted in a histogram. A Shannon entropy analysis of the orientation histogram was performed, providing information on whether collagen fibers exhibit a complex distribution of orientations or if a specific set of orientations predominate. Mean coherency of masked and contrast enhanced images was also quantified as a proxy for local organization (Figure 1B,C). OrientationJ was used to threshold all analyzed pixels to a minimum of 4% coherency and 2% energy prior to any parameter quantification, thereby binarizing images to remove pixels without tissue from analysis in order to eliminate small histological defects or fissures (Figure 1D). No effect on SHG signals in areas immediately adjacent to removed defects were apparent. In total, four parameters were collected per image. Mean intensity provided information on the net content and integrity of collagen in the image. Intensity entropy provided a measure of the variability of intensity (and thus collagen content) within a given image.

FIGURE 1 Imaging processing pipeline eliminated defects and allowed for morphometric analysis. A, Background subtracted second harmonic generation imaging (SHG) images were used to calculate mean SHG intensity and intensity entropy. B, Fibril direction was calculated in contrast enhanced images, which were coherency mapped, and mean coherency was calculated. C, Fibril direction was calculated in contrast enhanced images, which were orientation mapped. Orientation histogram was plotted using this orientation map. Entropy of this histogram was calculated to yield orientation entropy. D, SHG Images were binarized by energy and coherency, and this binary mask was utilized to eliminate histological defects (indicated with *) from all analyses

Orientation entropy measured the variability in total fiber directions per image and serves as a proxy for total structural complexity. Coherency quantified the degree to fiber orientation matched that of its neighbors and thus quantified orientation complexity at a local level.

2.5 | Statistical analysis

Two-way ANOVA determined effects of Thompson degeneration grade and IVD position on the SHG intensity with Tukey *post hoc* test and using Graphpad Prism 7. Univariable and multivariable linear regression determined the association between Rutges degeneration score and age as independent variables and quantitative SHG parameters as dependent variables, with separate analyses for each parameter and region. Multivariable linear regression analysis was used to assess if Rutges degeneration score and Age significantly predicted quantitative SHG variables. An additional multivariable linear regression analysis was used to test if Rutges degeneration score and sex independently were associated with quantitative SHG values. All regression analyses were performed using R studio. Results are presented as mean ± SD. All error bars shown are one SD. Significance threshold was set at $P < .05$.

3 | RESULTS

### 3.1 | Degenerative processes are visible on SHG

Each of the PR/AB stained samples (Figure 2A) was used to determine imaging locations using the protocol discussed above, and SHG images were taken at midline (Figure 2B). SHG images were compiled into an array organized by image position. These positions were grouped into identifying zones (aAF, aT, NP, pT, and pAF) for both quantitative and morphological analysis (Figure 2C). Arrays from low Thompson grade IVDs (Thompsons grade 1 and 2) tended to show obvious lamellar structure in the aAF and pAF, and AF images were thus more morphologically distinct from NP images than in grade 4 and 5 IVDs.

Within the healthy NP, areas of uniform SHG intensity were observed, with structural elements taking on a fibrillar mesh-like appearance. However, as IVD degeneration progressed, bright structural elements within the NP were more commonly seen, which were found to be organized in a more linear fashion (Figure 3). Within the AF on the other hand, intensity did not grossly change with degeneration, but lamellar structure and fine structural elements such as interlamellar cross-bridges were more difficult to discern in degenerated IVDs. Collagen crimping as well as alternating lamellar layers were seen more prominently in healthy AF than in degenerated samples (Figure 3).
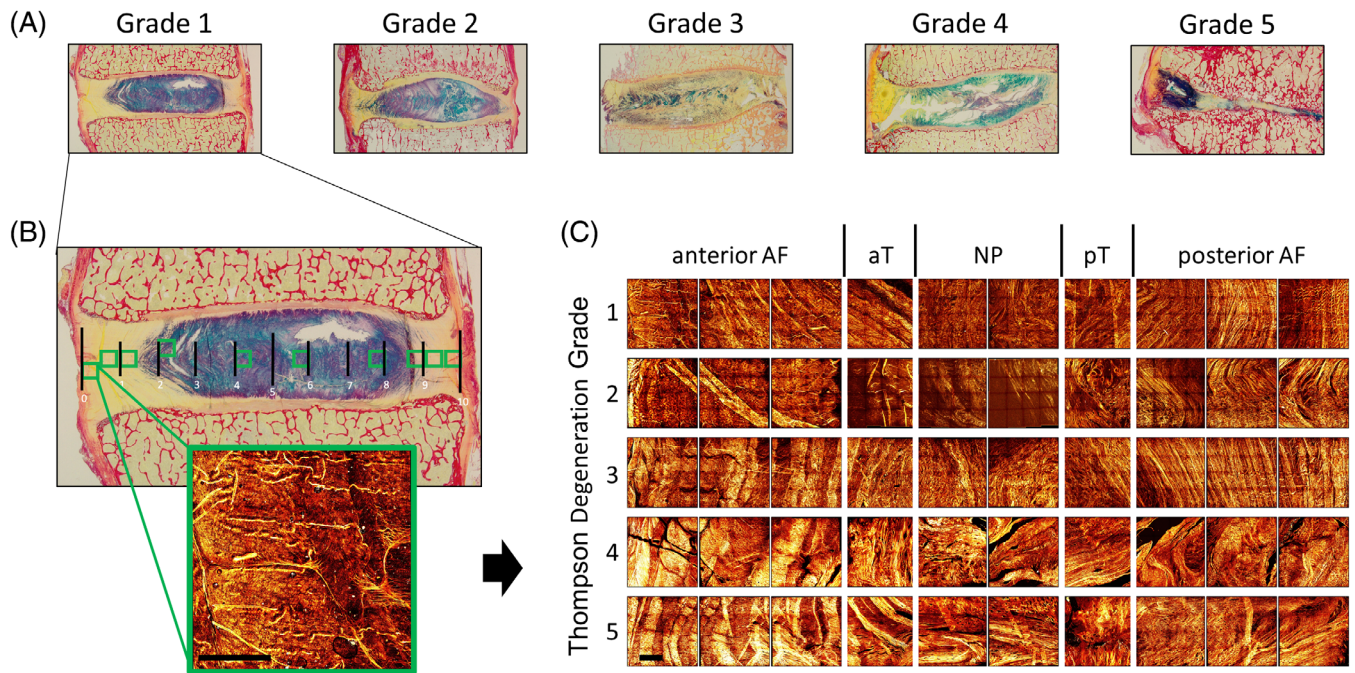
FIGURE 2 Second harmonic generation imaging (SHG) imaging and binning performed on 23 human IVDs at various degeneration grades. A, Mid-sagittal sections of lumbar L2/3 or L3/4 IVDs ranging from grade 1 to 5 on the Thompson degeneration scale (grade) were stained with PR/AB. B, Stained samples were imaged systematically at midline as indicated. C, Image arrays were compiled anterior to posterior. Binning into anterior AF (aAF), anterior transition zone (aT), NP, posterior transition zone (pT), and posterior AF (pAF) was defined as shown. Scale bar = 500 μm
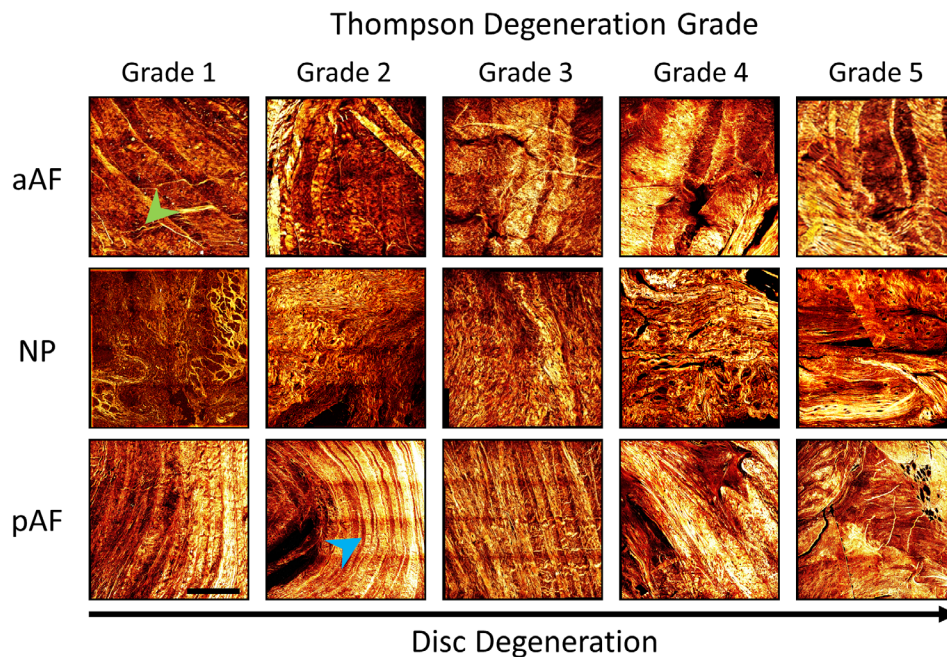
FIGURE 3 Degenerated NP showed more brightness variability on SHG, and both NP and AF demonstrated loss of visible microstructure on degeneration. Healthy NP (Thompson grades 1 and 2), demonstrated uniform dim signal, with fine collagenous mesh visible. Degenerated NP (Thompson grades 4 and 5) demonstrated bright linear formations, and loss of the fine collagenous mesh. Healthy anterior AF (aAF) and posterior AF (pAF) demonstrated discernable fine collagenous structure elements such as collagen crimping (green arrow), and alternating ply directions (blue arrow). Degenerated AF demonstrated loss of organization into lamella, and loss of all fine structural elements. SHG intensity was grossly unchanged. Scale bar = 500 μm

3.2 | SHG intensity increases in degenerated NP

SHG intensity exhibited distinct patterns with Thompson degeneration grade and this varied with region (Figure 4A). The Thompson grade was useful for the initial sorting of samples as it is based on gross observation and requires no sample processing. Thompson grade 1 and 2 samples exhibited SHG intensity that was lowest in the NP regions while grades 3 to 5 exhibited SHG intensity patterns that were flatter across regions from aAF to NP and pAF. On analysis, significant interaction between Thompson grade and IVD position was seen on two-way ANOVA when considering imaging positions independently (interaction $P = .0463$, 14.85% of variation; IVD position $P < .0001$, 22.2% of variation; Thompson Grade $P = .0119$, 1.63% of variation), yet the Thompson effect on intensity did not persist upon post hoc analysis at individual positions. The Rutges histological grading scale was used for all further correlation analysis with SHG imaging parameters because it has greater resolution and accounts for microscopic changes, as specimens are graded based on detailed observations of histological sections rather than from observations of images of gross morphology used for Thompson grading. Confirming that both scales measure degeneration, Thompson morphological grading score was strongly correlated with Rutges histological grading score (Figure 4B). Increasing SHG intensity was significantly correlated with increasing Rutges grade within the NP, and the pT. Intensity changes at the aAF, aT, and pAF were not significantly correlated with degeneration (Figure 4C).

3.3 | Morphometric analysis indicates loss of signal complexity with degeneration

Both SHG intensity entropy and orientation entropy showed regional decline with degeneration, indicating loss of variability in collagen content and organizational complexity with degeneration. SHG intensity entropy significantly decreased with Rutges degeneration grade in the aAF and pAF (Figure 5A). No significant effect on SHG intensity entropy was found within the aT, NP, or pT. SHG orientation entropy decreased significantly in most regions of the IVD: aAF, aT, NP, and
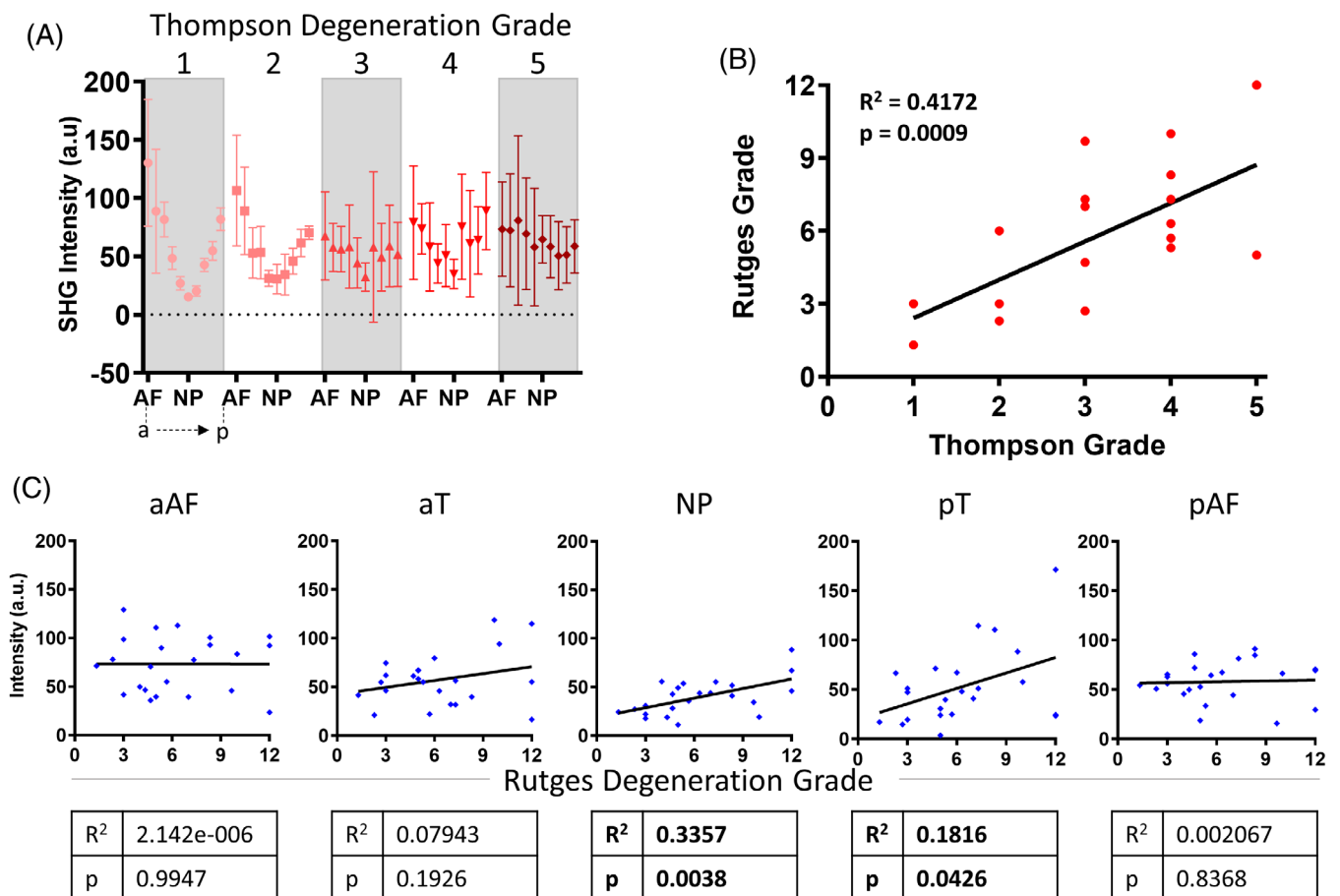
FIGURE 4 Second harmonic generation imaging (SHG) intensity is affected by Thomson grade and Rutges Grade in the NP and PT. A, SHG intensity was plotted by IVD position, anterior (a) to posterior (p), and by Thompson grades 1–5. Error bars are one SD. B Rutges and Thompson degenerative scales significantly correlated with each other. C SHG intensity compared to Rutges score in all regions of the IVD. Analysis shown anterior to posterior. Correlations per region indicated at bottom
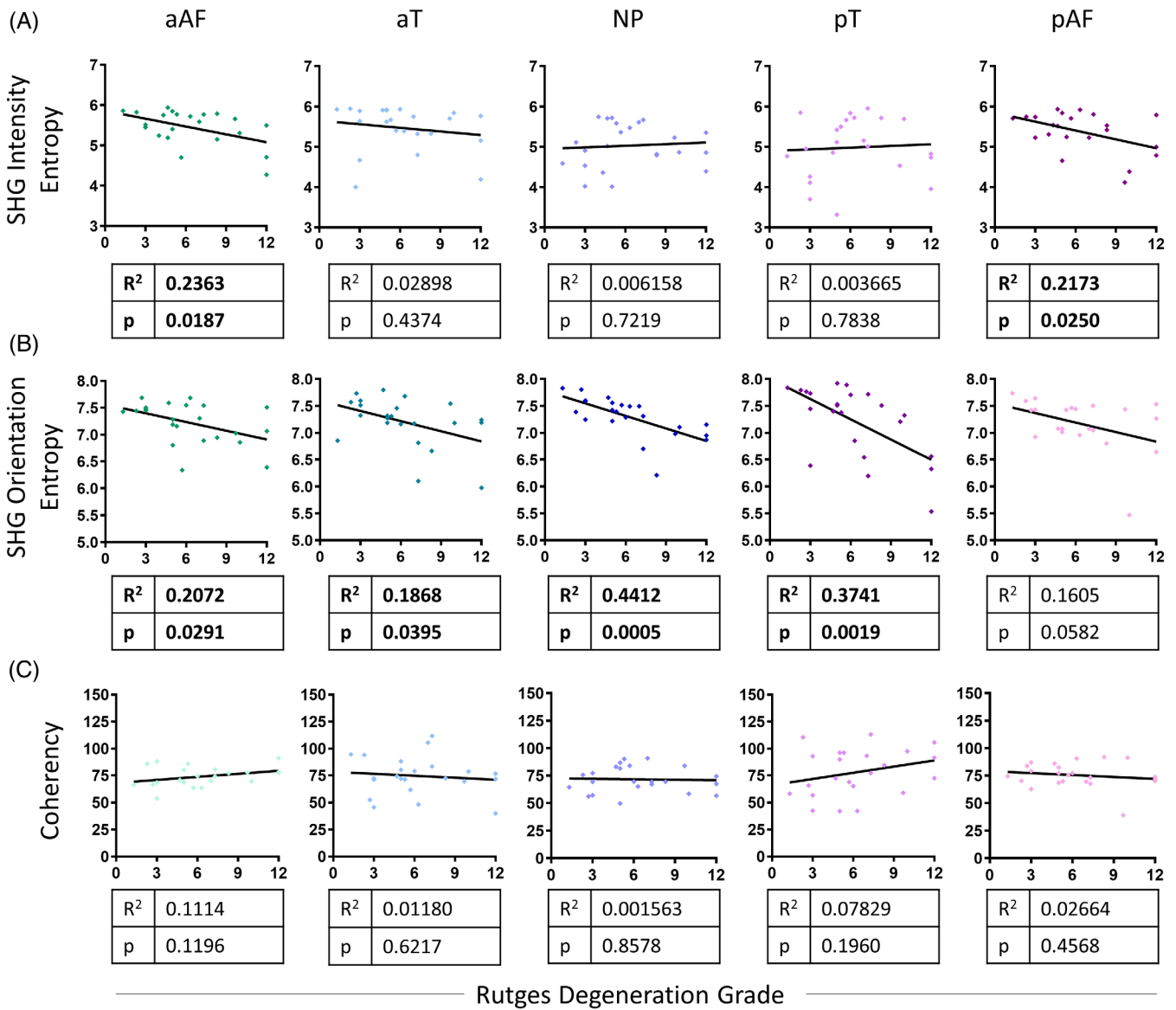
FIGURE 5 Second harmonic generation imaging (SHG) intensity entropy decreases in the aAF and pAF with degeneration. Orientation entropy decreases broadly with degeneration. Correlation of Rutges degeneration grades to, A, SHG intensity entropy, B, orientation entropy and, C, coherency across the IVD from anterior to posterior. Correlations per region indicated under each graph with aAF = anterior AF, aT = anterior transition zone, pT = posterior transition zone and pAF = posterior AF

FIGURE 6 Rutges and Thompson degeneration grades both correlate with age. A, Sample age significantly correlated with Thompson grade and, B Rutges grade. Correlation indicated in each graph
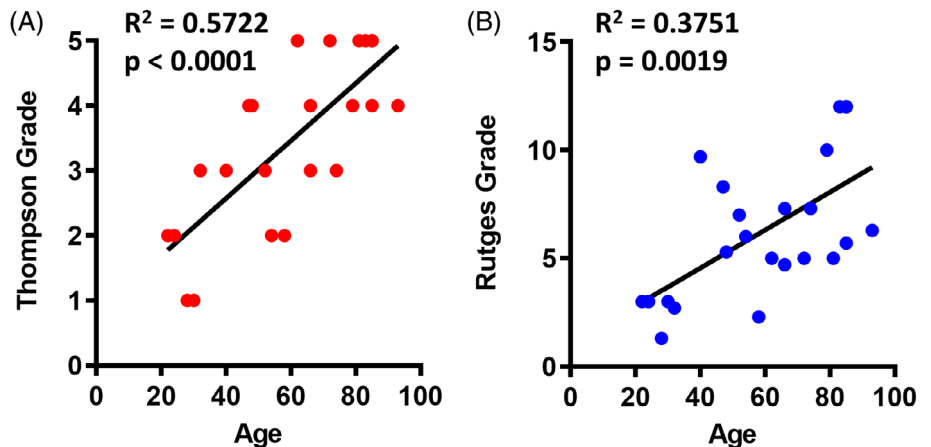
TABLE 2 Multiple regression results assessing contributions of degeneration and aging. Only areas showing $P < .05$ for linear regression with Rutges degeneration grade could be included in multiple regression analysis

			aAF	aT	NP	pT	pAF
SHG Intensity	Linear regression		$P = .9947$	$P = .1926$	**$P = .0038$**	**$P = .0426$**	$P = .8368$
	Multiple regression	Rutges			**$P = .0357$**	$P = .3$	
		Age			$P = .5521$	$P = .164$	
		Overall			**$P = .01108$**	**$P = .035$**	
		R^2			0.2988	0.2133	
Intensity Entropy	Linear regression		**$P = .0187$**	$P = .4374$	$P = .7219$	$P = .7838$	**$P = .0250$**
	Multiple regression	Rutges	$P = .25$				**$P = .0193$**
		Age	$P = .08$				$P = .3499$
		Overall	**$P = .009161$**				**$P = .0487$**
		R^2	0.312				0.1869
Orientation Entropy	Linear regression		**$P = .0291$**	**$P = .0395$**	**$P = .0005$**	**$P = .0019$**	$P = .0582$
	Multiple regression	Rutges	$P = .214$	$P = .0714$	**$P = .00085$**	**$P = .0061$**	
		Age	$P = .371$	$P = .7411$	$P = .298$	$P = .6128$	
		Overall	$P = .06509$	$P = .1196$	**$P = .001665$**	**$P = .00809$**	
		R^2	0.163	0.1104	0.4199	0.3205	
Coherency	Linear regression		$P = .1196$	$P = .6217$	$P = .8578$	$P = .1960$	$P = .4568$
	Multiple regression	Rutges					
		Age					
		Overall					
		R^2					

Abbreviations: AF, annulus fibrosus; aAF, anterior AF; NP, nucleus pulposus; pAF, posterior AF; SHG, second harmonic generation imaging.

pT (Figure 5B). Orientation entropy of the pAF decreased with Rutges degeneration score, but this trend was not significant ($P = .0582$, $R^2 = 0.1605$) (Figure 5B). Coherency was not significantly correlated with degeneration grade in any region (Figure 5C).

3.4 | Degeneration correlates with age, not sex

Both the Thompson ($P < .0001$, $R^2 = 0.5722$) and Rutges degeneration ($P = .0019$, $R^2 = 0.3751$) grades correlated with sample age (Figure 6A,B).

Due to the correlation between age and degeneration, SHG measurements that were identified to be significantly affected by Rutges grade were also analyzed via multivariable linear regression using age as a covariate. This was done to determine whether degeneration effects were age-independent. While adjusting for age as a covariate, Rutges remained independently associated with (a) SHG intensity in the NP, (b) intensity entropy in the pAF, and (c) orientation entropy in the NP and pT (Table 2). Of note, variance inflation factors indicated that multicollinearity was not a concern. An absence of degeneration-independent effects of age on SHG parameters suggested that we can interpret our reported alterations in SHG variables as degeneration-related changes.

An additional multiple regression used sex and Rutges degeneration grade as a covariate. Sex was not significantly associated with any of the SHG parameters measured (NP intensity, $P = .405$; pT intensity, $P = .1845$; aAF intensity entropy, $P = .131$; pAF intensity entropy, $P = .0922$; aAF orientation entropy, $P = .2441$; aT orientation entropy, $P = .798$; NP orientation entropy, $P = .112$; pT orientation entropy, $P = .61287$).

4 | DISCUSSION

In this study, we analyzed SHG intensity and various morphometric parameters at various degeneration grades. We observed an increase in NP signal intensity with degeneration, and a decrease in both intensity entropy and orientation entropy within the AF. Taken together, these results suggest fibrotic collagen deposition in the NP, and a loss of structural complexity of collagen in the AF with degeneration.

SHG morphometric analysis indicated a loss of structural complexity with degeneration including increased fibrosis and a loss of large features like lamellae. Multiple morphometric properties of the IVD were used to identify changes that occur in degeneration. Shannon entropy was used to quantify the randomness of intensity, as a proxy for the uniformity of collagen structure within the analyzed frame.[39] Although quantitative validation of intensity entropy has not been performed within the IVD, its implications regarding image composition are well established,[39] and entropy has been shown to decrease as collagenous tissues become more uniform from processes

such as collagen deposition[40] and fibrosis[41] using other imaging modalities. A loss in intensity entropy suggests a decrease in variability of intensity throughout the image, with more uniformity in where collagen is present and organized. We therefore interpret the decrease in intensity entropy with degeneration in aAF and pAF regions to indicate that fibrosis in the AF has caused the loss of distinct structures like alternating lamellar layers, leading to a shift towards a more uniform image field. We utilized OrientationJ in our morphometric analysis, a plugin based on structure tensors that evaluates the local orientation and isotropic properties (orientation, coherency, and energy) of every pixel in the image.[38] It has been used extensively to quantify collagen orientation and disorder.[39,42,43] Quantifying the entropy of the resulting orientation map provides a measure of the complexity of collagen orientations in the imaged structure. We interpret the significant reduction in orientation entropy with degeneration in nearly all IVD regions to quantify the loss of structural features across the IVD. Coherency describes the degree to which pixels share their orientation with their neighbors, with high coherency indicating low variability in orientation at a local level.[22] The significant reduction in orientation entropy with degeneration, combined with no alterations in coherency, suggests loss of the image-wide structural complexity of collagen with disruption of larger scale features like lamellae through fibrosis, without distortion at the local level. We interpret the lack of change in coherency to suggest that both the original and the newly deposited fibrils remain structurally intact at the 2-pixel scale. While this can indicate that individual fibrils remain intact, no specific molecular changes at this scale were detected.

SHG alterations pointed toward increased NP fibrosis since SHG intensity increased within the NP and adjoining pT with degeneration and there was a qualitative shift from predominantly fine fibrillar network to linear structural features with high SHG intensity. Previous research suggested a shift from type II collagen to type I collagen content as the NP degenerates,[13,18,19] with a concurrent decrease in total collagen content.[18,44] The loss in total collagen stands in contrast to the notable morphological shift from gelatinous to fibrous that is often described in the literature.[17,45] Collagen type I and II have been discerned with SHG due to the greater polarity in collagen type I that results in higher SHG signal on average,[46] although it was impossible to determine collagen type quantitatively in our human IVD samples using SHG due to high local variability in collagen concentrations and orientations. We did observe a quantitative increase in SHG signal intensity and a qualitative increase in larger collagenous structures in the NP and note the literature that shows a decrease in collagen content and shift from collagen type II to type I in the NP with degeneration.[13,18,19] We infer increased fibrotic deposition in the NP is most likely related to accumulation of type I collagen. SHG can therefore identify alterations in NP collagen with degeneration.

The reduced intensity entropy and orientation entropy with degeneration in the AF indicated a loss of micro-structural features. Loss of the counter-oblique collagen orientation, interlamellar cross-bridges, and collagen crimping were previously reported,[33,47] and all observed to be diminished in degenerated IVDs in our study. Loss of

microstructural components can contribute to a decrease in structural integrity of the AF,[48] and this mechanical damage accumulates in the IVD during degeneration.[49] Furthermore, the loss of orientation entropy could be associated with the microfailure of the AF inter-lamellar matrix, which was shown to be the weakest AF structure prone to microfailure under high loading conditions.[50] We note that, to our knowledge, a comparison of type I and type II collagen has not been performed in terms of their effects on intensity entropy, thus we cannot make compositional assumptions based on these data. The healthy AF has greater orientation entropy, even in the NP, indicating a greater number of families of fibers with varying orientations. The observed decrease in orientation entropy change indicates that the degenerated IVD structures have collagen with fewer families of fiber orientations. The loss of orientation entropy may therefore suggest that molecular degradation of the original collagen occurs and is replaced with new collagen that takes on a simpler configuration. This would not be surprising given evidence of inflammatory processes within the AF and NP in degeneration.[51-53]

The increased structural homogeneity identified in degenerated IVDs in this study is similar to previous studies on the AF including SHG analyses. Comparing collagen fiber orientation distributions in moderately degenerated IVD as measured with SHG[27] with previous work showing larger differences in fiber orientation in healthy AF[11] together suggested the concept that degeneration causes the AF structure to become more homogeneous. Our finding confirms this observation by quantitatively showing that AF orientation entropy decreases with degeneration. Our qualitative observation that crimping decreased with degeneration may also suggest that the observed lack of crimping in adult human IVDs when compared to young bovine IVD on SHG is likely a degenerative change rather than a species difference, as hypothesized by Vergari et al.[33]

SHG intensity provided a robust measure of collagen organization and its alterations with degeneration but is limited since pain can not be assessed. While structural IVD changes are known to correlate with pain, this study on cadaveric IVDs does not include knowledge of clinical back pain symptoms. While SHG intensity is affected by multiple parameters, including collagen fibril diameter, content, and molecular integrity, the morphometric analyses are not affected by these alterations in those parameters. We controlled for histological defects by binarizing our images and removing the pixels from large defects due to histological processing or fissures and results therefore compare the collagen matrix across degeneration grades. Since the number of defects increases with degeneration, we note severely degenerated IVDs would have an increase in structural disruptions in addition to the collagen network changes described in this SHG study. The fibrosis hypothesis presented suggests that the original collagenous structure within the AF degenerates and is replaced with new collagen, and future studies can assess degenerated collagen using collagen hybridizing peptide as a probe.[54-56] Lastly, future SHG analysis concurrent with biomechanical experiments may further elucidate structure-function relationships since structural changes in collagen are expected upon load application.[49,57-59]

In conclusion, this study applied SHG imaging and multiple image processing algorithms to quantify the spatial changes in collagen structure with IVD degeneration. SHG intensity increased in the NP with degeneration, demonstrating greater quantity of organized collagen. We conclude that this increased intensity and qualitative alteration demonstrates altered collagen fiber structure, and in the context of the literature, suggests fibrotic deposition of larger collagen structures likely involving type I collagen accumulation. Intensity entropy decreased in the AF and orientation entropy decreased throughout the IVD with degeneration, highlighting a loss of structural complexity. We posit that this loss of structural complexity with human IVD degeneration resulted from the replacement of healthy collagen consisting of complex structural features with fibrotic collagen of simpler organization. These alterations were distinguished from aging changes. These IVD structural changes with degeneration suggest a loss of structural integrity and highlight a need for future studies characterizing micro-injury and healing processes.

CONFLICT OF INTEREST

None.

AUTHOR CONTRIBUTIONS

Lawrence Zeldin contributed to project design, prepared samples, performed SHG imaging and analysis, contributed to statistical analysis, interpreted results, and wrote the manuscript. Grace E. Mosley contributed to project design, interpreted results, and contributed to manuscript writing. Damien M. Laudier prepared human sections for study and assisted with histological imaging. Zachary S. Gallate performed sample preparation, histological imaging, Rutges grading, and contributed to statistical analysis. Jennifer Gansau assisted with figure creation and contributed to manuscript writing. Robert C. Hoy contributed to the SHG imaging and analysis pipeline and interpretation of results. Jashvant Poeran contributed to statistical analysis and interpretation. James C. Iatridis initiated the project and contributed to experimental design, interpretation of results, and manuscript writing. All authors reviewed the manuscript.

ORCID

Lawrence Zeldin https://orcid.org/0000-0002-3953-219X
Grace E. Mosley https://orcid.org/0000-0002-8971-8080
Zachary S. Gallate https://orcid.org/0000-0001-7512-9122
Jennifer Gansau https://orcid.org/0000-0002-1951-2933
Robert C. Hoy https://orcid.org/0000-0001-9000-5793
Jashvant Poeran https://orcid.org/0000-0001-7058-5102
James C. Iatridis https://orcid.org/0000-0002-2186-0590

REFERENCES

1. Vos T, Flaxman AD, Naghavi M, et al. Years lived with disability (YLDs) for 1160 sequelae of 289 diseases and injuries 1990–2010: a systematic analysis for the global burden of disease study 2010. *Lancet*. 2012;*380*(9859):2163-2196.
2. Andersson GB. Epidemiological features of chronic low-back pain. *Lancet*. 1999;*354*(9178):581-585.
3. Freburger JK, Holmes GM, Agans RP, et al. The rising prevalence of chronic low back pain. *Arch Intern Med*. 2009;*169*(3):251-258.
4. Hartvigsen J, Hancock MJ, Kongsted A, et al. What low back pain is and why we need to pay attention. *Lancet*. 2018;*391*(10137):2356-2367.
5. Rubin DI. Epidemiology and risk factors for spine pain. *Neurol Clin*. 2007;*25*(2):353-371.
6. Ravindra VM, Senglaub SS, Rattani A, et al. Degenerative lumbar spine disease: estimating global incidence and worldwide volume. *Global Spine J*. 2018;*8*(8):784-794.
7. Luoma K, Riihimaki H, Luukkonen R, Raininko R, Viikari-Juntura E, Lamminen A. Low back pain in relation to lumbar disc degeneration. *Spine (Phila pa 1976)*. 2000;*25*(4):487-492.
8. Eyre DR, Muir H. Types I and II collagens in intervertebral disc. Interchanging radial distributions in annulus fibrosus. *Biochem J*. 1976;*157*(1):267-270.
9. Roughley PJ. Biology of intervertebral disc aging and degeneration: involvement of the extracellular matrix. *Spine (Phila pa 1976)*. 2004;*29*(23):2691-2699.
10. Yu J, Tirlapur U, Fairbank J, et al. Microfibrils, elastin fibres and collagen fibres in the human intervertebral disc and bovine tail disc. *J Anat*. 2007;*210*(4):460-471.
11. Cassidy JJ, Hiltner A, Baer E. Hierarchical structure of the intervertebral disc. *Connect Tissue Res*. 1989;*23*(1):75-88.
12. Wei Y, Tower RJ, Tian Z, et al. Spatial distribution of type II collagen gene expression in the mouse intervertebral disc. *JOR Spine*. 2019;*2*(4):e1070.
13. Antoniou J, Steffen T, Nelson F, et al. The human lumbar intervertebral disc: evidence for changes in the biosynthesis and denaturation of the extracellular matrix with growth, maturation, ageing, and degeneration. *J Clin Invest*. 1996;*98*(4):996-1003.
14. Iatridis JC, MacLean JJ, O'Brien M, Stokes IA. Measurements of proteoglycan and water content distribution in human lumbar intervertebral discs. *Spine (Phila pa 1976)*. 2007;*32*(14):1493-1497.
15. Bezci SE, Werbner B, Zhou M, et al. Radial variation in biochemical composition of the bovine caudal intervertebral disc. *JOR Spine*. 2019;*2*(3):e1065.
16. Buckwalter JA. Aging and degeneration of the human intervertebral disc. *Spine (Phila pa 1976)*. 1995;*20*(11):1307-1314.
17. Haefeli M, Kalberer F, Saegesser D, Nerlich AG, Boos N, Paesold G. The course of macroscopic degeneration in the human lumbar intervertebral disc. *Spine (Phila pa 1976)*. 2006;*31*(14):1522-1531.
18. Singh K, Masuda K, Thonar EJ, An HS, Cs-Szabo G. Age-related changes in the extracellular matrix of nucleus pulposus and anulus fibrosus of human intervertebral disc. *Spine (Phila pa 1976)*. 2009;*34*(1):10-16.
19. Kaapa E, Han XY, Holm S, Peltonen J, Takala T, Vanharanta H. Collagen-synthesis and type-i, type-iii, type-iv, and type-vi collagens in an animal-MODEL of disc degeneration. *Spine*. 1995;*20*(1):59-66.
20. Yoon ST. Molecular therapy of the intervertebral disc. *Spine J*. 2005;*5*(6 Suppl):280S-286S.
21. Stoller P, Reiser KM, Celliers PM, Rubenchik AM. Polarization-modulated second harmonic generation in collagen. *Biophys J*. 2002;*82*(6):3330-3342.
22. Reiser KM, Bratton C, Yankelevich DR, Knoesen A, Rocha-Mendoza I, Lotz J. Quantitative analysis of structural disorder in intervertebral disks using second harmonic generation imaging: comparison with morphometric analysis. *J Biomed Opt*. 2007;*12*(6):064019.

23. Raub CB, Putnam AJ, Tromberg BJ, George SC. Predicting bulk mechanical properties of cellularized collagen gels using multiphoton microscopy. *Acta Biomater.* 2010;6(12):4657-4665.

24. Chen X, Nadiarynkh O, Plotnikov S, Campagnola PJ. Second harmonic generation microscopy for quantitative analysis of collagen fibrillar structure. *Nat Protoc.* 2012;7(4):654-669.

25. Campagnola P. Second harmonic generation imaging microscopy: applications to diseases diagnostics. *Anal Chem.* 2011;83(9):3224-3231.

26. Bancelin S, Aime C, Gusachenko I, et al. Determination of collagen fibril size via absolute measurements of second-harmonic generation signals. *Nat Commun.* 2014;5:4920.

27. Dittmar R, van Rijsbergen MM, Ito K. Moderately degenerated human intervertebral disks exhibit a less geometrically specific collagen fiber orientation distribution. *Global Spine J.* 2016;6(5):439-446.

28. Fine S, Hansen WP. Optical second harmonic generation in biological systems. *Appl Opt.* 1971;10(10):2350-2353.

29. Cicchi R, Vogler N, Kapsokalyvas D, Dietzek B, Popp J, Pavone FS. From molecular structure to tissue architecture: collagen organization probed by SHG microscopy. *J Biophotonics.* 2013;6(2):129-142.

30. Zipfel WR, Williams RM, Christie R, Nikitin AY, Hyman BT, Webb WW. Live tissue intrinsic emission microscopy using multiphoton-excited native fluorescence and second harmonic generation. *Proc Natl Acad Sci U S A.* 2003;100(12):7075-7080.

31. Cox G, Kable E, Jones A, Fraser I, Manconi F, Gorrell MD. 3-dimensional imaging of collagen using second harmonic generation. *J Struct Biol.* 2003;141(1):53-62.

32. Paietta RC, Burger EL, Ferguson VL. Mineralization and collagen orientation throughout aging at the vertebral endplate in the human lumbar spine. *J Struct Biol.* 2013;184(2):310-320.

33. Vergari C, Chan D, Clarke A, Mansfield JC, Meakin JR, Winlove PC. Bovine and degenerated human annulus fibrosus: a microstructural and micromechanical comparison. *Biomech Model Mechanobiol.* 2017;16(4):1475-1484.

34. Thompson JP, Pearce RH, Schechter MT, Adams ME, Tsang IK, Bishop PB. Preliminary evaluation of a scheme for grading the gross morphology of the human intervertebral disc. *Spine (Phila pa 1976).* 1990;15(5):411-415.

35. Walter BA, Torre OM, Laudier D, Naidich TP, Hecht AC, Iatridis JC. Form and function of the intervertebral disc in health and disease: a morphological and stain comparison study. *J Anat.* 2015;227(6):707-716.

36. Rutges JP, Duit RA, Kummer JA, et al. A validated new histological classification for intervertebral disc degeneration. *Osteoarthritis Cartilage.* 2013;21(12):2039-2047.

37. Schindelin J, Arganda-Carreras I, Frise E, et al. Fiji: an open-source platform for biological-image analysis. *Nature Methods.* 2012;9(7):676-682.

38. Rezakhaniha R, Agianniotis A, Schrauwen JT, et al. Experimental investigation of collagen waviness and orientation in the arterial adventitia using confocal laser scanning microscopy. *Biomech Model Mechanobiol.* 2012;11(3–4):461-473.

39. Wu Y, Zhou YC, Saveriades G, Agaian S, Noonan JP, Natarajan P. Local Shannon entropy measure with statistical tests for image randomness. *Inform Sci.* 2013;222:323-342.

40. Rocha LB, Adam RL, Leite NJ, Metze K, Rossi MA. Shannon's entropy and fractal dimension provide an objective account of bone tissue organization during calvarial bone regeneration. *Microsc Res Tech.* 2008;71(8):619-625.

41. Hao L, Tu JZ, Wang XH, Shi Y, Liu XL, Zhang HH. Effect of inflammation on fibrosis staging measured by quantitative elasticity parameters in rats with immune hepatitis. *J Ultrasound Med.* 2016;35(6):1223-1231.

42. Mosley GE, Hoy RC, Nasser P, et al. Sex differences in rat intervertebral disc structure and function following annular puncture injury. *Spine (Phila Pa 1976).* 2019;44(18):1257-1269.

43. Sampath SA, Lewis S, Fosco M, Tigani D. Trabecular orientation in the human femur and tibia and the relationship with lower-limb alignment for patients with osteoarthritis of the knee. *J Biomech.* 2015;48(6):1214-1218.

44. Vo NV, Hartman RA, Patil PR, et al. Molecular mechanisms of biological aging in intervertebral discs. *J Orthop Res.* 2016;34(8):1289-1306.

45. Iatridis JC, Setton LA, Weidenbaum M, Mow VC. Alterations in the mechanical behavior of the human lumbar nucleus pulposus with degeneration and aging. *J Orthop Res.* 1997;15(2):318-322.

46. Su PJ, Chen WL, Li TH, et al. The discrimination of type I and type II collagen and the label-free imaging of engineered cartilage tissue. *Biomaterials.* 2010;31(36):9415-9421.

47. Gruber HE, Hanley EN Jr. Observations on morphologic changes in the aging and degenerating human disc: secondary collagen alterations. *BMC Musculoskelet Disord.* 2002;3:9.

48. Masic A, Bertinetti L, Schuetz R, et al. Observations of multiscale, stress-induced changes of collagen orientation in tendon by polarized Raman spectroscopy. *Biomacromolecules.* 2011;12(11):3989-3996.

49. Tavakoli J, Amin DB, Freeman BJC, Costi JJ. The biomechanics of the inter-lamellar matrix and the lamellae during progression to lumbar disc herniation: which is the weakest structure? *Ann Biomed Eng.* 2018;46(9):1280-1291.

50. Videman T, Nurminen M. The occurrence of anular tears and their relation to lifetime back pain history: a cadaveric study using barium sulfate discography. *Spine (Phila pa 1976).* 2004;29(23):2668-2676.

51. Nakazawa KR, Walter BA, Laudier DM, et al. Accumulation and localization of macrophage phenotypes with human intervertebral disc degeneration. *Spine J.* 2018;18(2):343-356.

52. Purmessur D, Walter BA, Roughley PJ, Laudier DM, Hecht AC, Iatridis J. A role for TNFalpha in intervertebral disc degeneration: a non-recoverable catabolic shift. *Biochem Biophys Res Commun.* 2013;433(1):151-156.

53. Weiler C, Nerlich AG, Zipperer J, Bachmeier BE, Boos N. 2002 SSE award competition in basic science: expression of major matrix metalloproteinases is associated with intervertebral disc degradation and resorption. *Eur Spine J.* 2002;11(4):308-320.

54. Hwang J, Huang Y, Burwell TJ, et al. In situ imaging of tissue remodeling with collagen hybridizing peptides. *ACS Nano.* 2017;11(10):9825-9835.

55. Hwang J, San BH, Turner NJ, et al. Molecular assessment of collagen denaturation in decellularized tissues using a collagen hybridizing peptide. *Acta Biomater.* 2017;53:268-278.

56. Xiao L, Majumdar R, Dai J, et al. Molecular detection and assessment of intervertebral disc degeneration via a collagen hybridizing peptide. *Acs Biomater Sci Eng.* 2019;5(4):1661-1667.

57. Ruspi ML, Palanca M, Cristofolini L, et al. Digital image correlation (DIC) assessment of the non-linear response of the anterior longitudinal ligament of the spine during flexion and extension. *Materials (Basel).* 2020;13(2):384. https://doi.org/10.3390/ma13020384.

58. Palanca M, Ruspi ML, Cristofolini L, et al. The strain distribution in the lumbar anterior longitudinal ligament is affected by the loading condition and bony features: An in vitro full-field analysis. *PLoS One.* 2020;15(1):e0227210.

59. Lynch HA, Johannessen W, Wu JP, Jawa A, Elliott DM. Effect of fiber orientation and strain rate on the nonlinear uniaxial tensile material properties of tendon. *J Biomech Eng.* 2003;125(5):726-731.